Two dimension structured surfaces

Contents

1 Introduction

The benefits of structured surfaces have been known for long. However, since the origin of their discovery, experimental and theoretical studies focused on two dimension structures mostly for simplicity reasons. The drag reduction of these structures may reach 10 – 12 % in the most favourable situation (optimised shape with both optimised height and spacing). Economics carried out on 30 year operation pipelines have shown the same order of magnitude of cost reduction by applying structured surfaces on the surface of pipe internal coatings despite it may vary slightly with the operating case.

According to some publications and several patents, the flow drag could be reduced further by using three dimensional structures with increased saving in capital and operating costs. Considering the large energy dissipation attributed to turbulence at large Reynolds number (99% due to turbulence for only 1% due to viscosity), significant drag reduction could be obtained by using more optimised / sophisticated structures. Experimental studies would be extremely difficult to carry out considering the large number of unknown parameters. Theoretical studies are nowadays more accessible due to considerable progress in computers and software’s. Three types of Computational Fluid Dynamics codes (DNS, RANS, LES) are now available for studying the turbulence development near a wall or in the flow core and therefore for predicting, relatively accurately, energy dissipation. An evaluation of CFD codes is presented in this section together with flow simulations (RANS in this section and LES in the next section) based on two techniques of drag reduction.

2_Generalities on structured surfaces

2.1_Description – Principle of operation

Organised structures forming grooves aligned in the flow direction (figure 2.1) present the characteristic of reducing the flow drag. This drag reduction results from an attenuation by the grooves of the propagation of the transverse component of local velocity fluctuations (figure 2.2). When dimensions of solid organised structures are adapted to dimensions of stream wise (longitudinal) vortices (figure 2.2.b) the flow drag is reduced compared to a flat surface (figure 2.2.a) due to a reduction in both the friction area and the displacement of transverse fluctuating flow velocities. When dimensions of solid organised structures are larger than dimensions of stream wise vortices (figure 2.2.c) the flow drag reduction is limited due to the entrance of these vortices within the solid structures causing an increase in friction area. When dimensions and shape of solid organised structures are further adapted to turbulent structures (figure 2.2.d) the flow drag is reduced to its maximum: largest reduction in friction area with largest limitation in transmission of transverse turbulence.

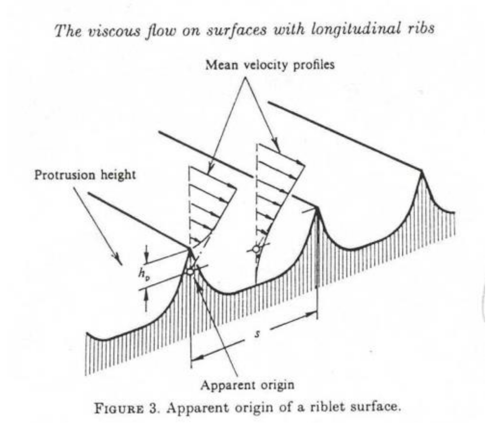

Figure 2.1 – Two dimension structures (riblets) aligned in the flow direction. Diagram by D.Bechert (1989)

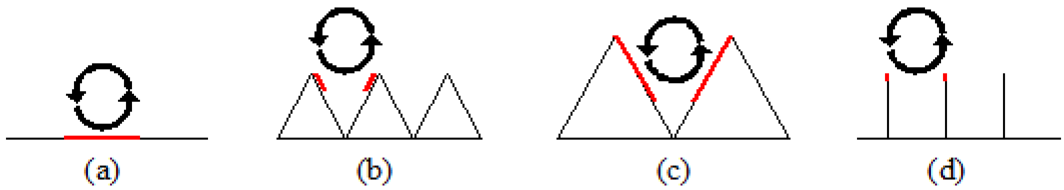

Figure 2.2 – Principle of operation of structured surfaces. Turbulent structure (streamwise vortex) over a) a smooth surface, b) triangular riblets with adapted dimensions, c) triangular riblets with too large dimensions, d) knife blade riblets with adapted shape and dimensions

2.2_Types of structured surfaces

2.2.1 Two dimension surfaces

Two dimension structures present a constant height in the flow direction. Dimensions vary only in the transverse plane (perpendicular to the flow direction). Some examples of two dimension shapes are provided on figure 2.3 (a-triangular, b-semi-circular or scalloped shape, c-trapezoidal and d- knife blade shape).

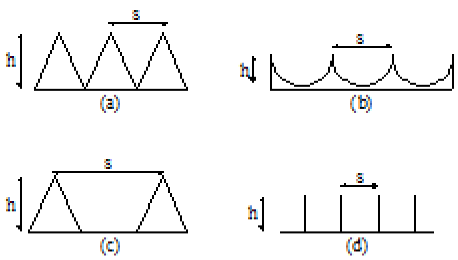

Figure 2.3 – Cross section of some types of two dimension structures

The drag reduction of 2D triangular riblets is of the order of 5 to 7%. The flow drag tends to reduce as the concavity of the groove is increased, reaching 10 to 12 % in the case of knife blade riblets.

2.2.2 Three dimension surfaces

According to some documents (publications and patents), the flow drag reduction would be significantly improved when using three dimension structures (figure 2.4.a to c).

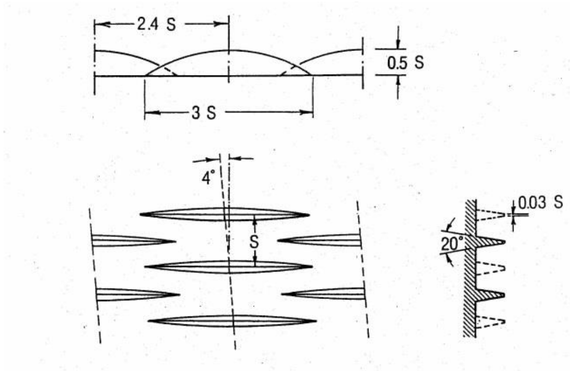

Fig.1: Configuration of the three-dimensional riblets

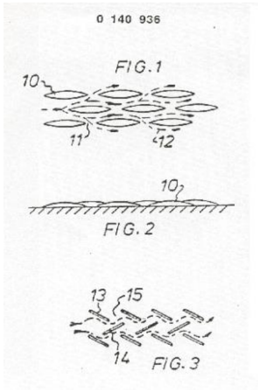

Figure 2.4.a – Three dimension structures by D.Bechert (1987) and Malstrom (1984)

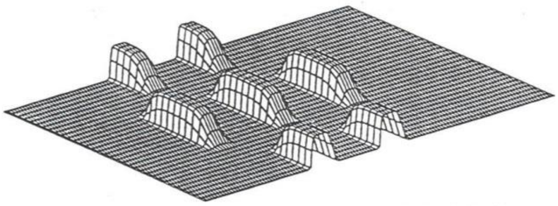

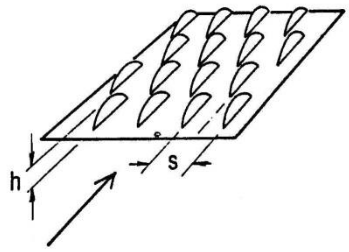

Figure 2.4.b - Three dimension structures by H.Choi (Humplets-1993) and D.Bechert (1987)

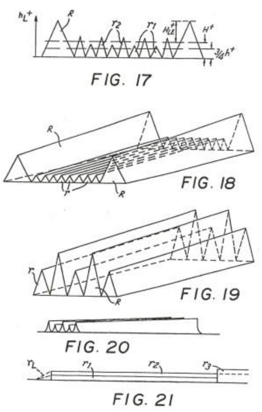

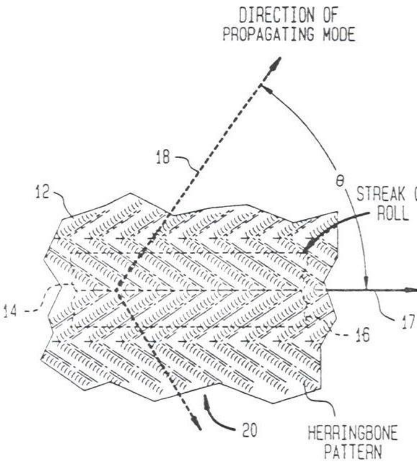

Figure 2.4.c – Complex two dimension structures by Savill (left_1995) and three dimension structures (chevron type) by Ormat (right_1992)

According to their authors, these structures would permit the reduction of normal and longitudinal velocity fluctuations in addition to the reduction of fluctuations in the transverse direction.

2.3_Optimum dimensions

Two dimension grooves provide a maximum flow drag reduction when their dimension (width and height) is approximately equal to 3 to 5 times the viscous layer thickness (based on 5 times the friction length). The optimised dimension is therefore mostly dependent on the fluid density, velocity and absolute viscosity, i.e., roughly, on the Reynolds number / pipe diameter ratio.

Structured surfaces for natural gas			
Pressure bar abs	Velocity-m/s	Viscous layer - µm	Structure dim. - µm
70	4	10 to 15	30 to 50
120	5.5	7 to 10	20 to 35
180	7	3 to 5	10 to 15

For gas transport, optimum dimensions range in between 50 and 10 µm depending on actual gas density and flow velocity.

2.4_Performance of structured surfaces

As mentioned in the above paragraph, a maximum flow drag reduction is obtained when an optimum flow (fixed dimension) or an optimum dimension (fixed flow) is met.

As the flow is reduced or increased from this optimised condition, the flow drag reduction tends progressively towards 0. The flow drag reduction is nil when the actual flow is approximately twice the optimum flow (figure 2.5).

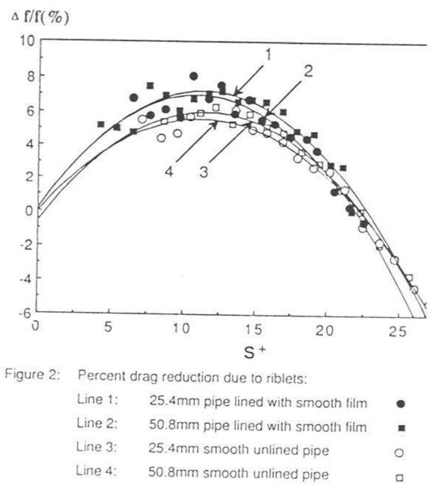

Figure 2.5 – Typical drag reduction of a triangular riblet– experimental results by K. N. Liu (1986)

The flow drag is reduced when the concavity of riblets is increased, as shown on figure 2.6 and comparing successively triangular, scalloped and knife blade riblets. Relative dimensions of riblets (width-S and height-H) need also to be adapted to get maximum drag. According to figure 2.6, adaptation is achieved with triangular, scalloped and knife blade riblets when H/S is approximately, respectively, 0.8, 0.7 and 0.5.

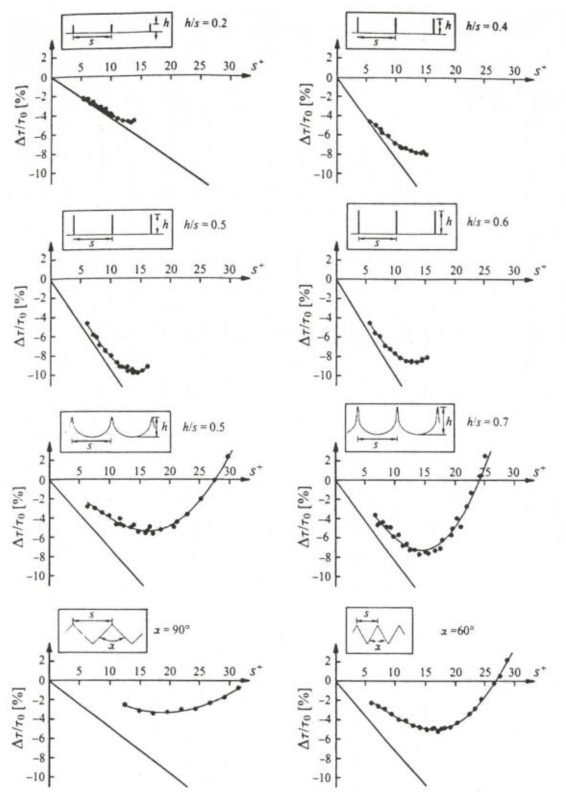

Figure 2.6 – Drag reduction for different types of riblets (blade knife, scalloped and triangular shapes) with different height / width ratios. Experimental results by D.Bechert (1997).

3_Computational Fluid Dynamics (CFD) codes

Turbulent flows are characterized by fluctuating velocity fields. These fluctuations cause transported quantities such as momentum and energy to fluctuate as well. Since these fluctuations can be of small scale and high frequency, they are too computationally expensive to simulate directly practical engineering cases (high Reynolds number). Instead, the instantaneous (exact) governing equations can be time-averaged or manipulated to remove the small scales, resulting in a modified set of equations that are computationally less expensive to solve. However, the modified equations contain additional unknown variables and turbulence models are needed to determine these variables in terms of known quantities.

Reynolds Averaged Navier-Stokes (RANS) equations represent transport equations for the mean flow quantities only, **with all the scales of the turbulence being modeled**. The approach of permitting a solution for the mean flow variables greatly reduces the computational effort. If the mean flow is steady, the governing equations do not contain time derivatives and a steady-state solution can be obtained economically. A computational advantage is found in transient situations where the time step is determined by the global unsteadiness in the mean flow rather than by the turbulence. The Reynolds-averaged approach is generally adopted for practical engineering calculations using models such as Spalart-Allmaras, $k\!-\!\varepsilon$ and its variant, $k\!-\!\omega$ and the RSM.

Large Eddy Simulation (LES) provides an alternative approach in which **the large eddies are computed in a time-dependent simulation** that uses a set of “filtered” equations. Filtering is essentially a manipulation of the exact Navier-Stokes equations to remove only the eddies that are smaller than the size of the filter which is usually taken as the mesh size. Like Reynolds averaging, the filtering process creates additional unknown terms that must be modeled in order to achieve closure. Statistics of the mean flow quantities, which are generally of most engineering interest, are gathered during the time-dependent simulation. One advantage of LES is that, by modeling less of the turbulence (and solving more), the error induced by the turbulence model is reduced. It might be argued that it should be easier to find a "universal" model for the small scales tending to be more isotropic and less affected by the macroscopic flow features than the large eddies.

3.1_Direct Numerical Simulation – DNS

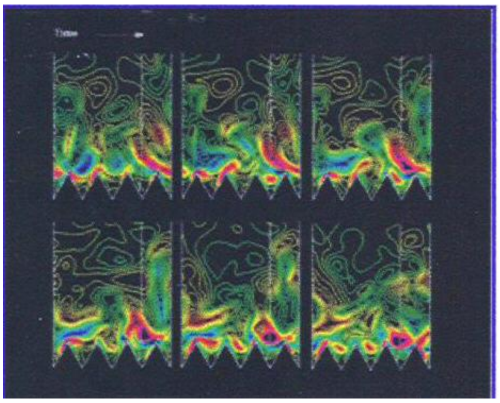

Figure 3.1 – Flow dynamics around triangular riblets_DNS calculation by Moin (1992).

Turbulent flows are characterized by eddies with a wide range of length and time scales. **The largest eddies are typically comparable in size to the characteristic length of the mean flow. The smallest scales are responsible for the dissipation of turbulence kinetic energy**. It is theoretically possible to directly resolve the whole spectrum of turbulent scales using an approach known as Direct Numerical Simulation (DNS). DNS is not, however, feasible for practical engineering problems (large Reynolds number).

To understand the large computational cost of DNS, it has to be considered that the ratio of the large (energy-containing) to the small (energy dissipating) scales is proportional to $Re_t^{3/4}$, where Re_t is the turbulent Reynolds number. Therefore, to resolve all the scales, the mesh size in three dimensions is proportional to $Re_t^{9/4}$. Simple arithmetic shows that, for high Reynolds numbers, the mesh number required for DNS is prohibitive. Adding to the computational cost is the fact that the simulation will be a transient one with very small time steps, since the temporal resolution requirements are governed by the dissipating (small) scales, rather than by the energy-containing (large) eddies.

Instant velocities may be written: $u_i = \overline{u_i} + u_i^{'}$ (3.1)

and scalar : $\phi = \overline{\phi} + \phi^{'}$ (3.2)

where the first and the second terms of the right hand side in both equations are, respectively, the mean and the fluctuant components.

In DNS, the following equations are directly resolved,

concerning the continuity equation by : $\frac{\partial p}{\partial t} + \frac{\partial}{\partial x_i}(\rho u_i) = 0$ (3.3)

and the momentum equation by :

$$\frac{\partial}{\partial t}(\rho u_i) + \sum_j \frac{\partial}{\partial x_j}(\rho u_i . u_j) = -\frac{\partial p}{\partial x_i} + \sum_j \frac{\partial}{\partial x_j}\left[\mu\left(\frac{\partial u_i}{\partial x_j} + \frac{\partial u_j}{\partial x_i} - \frac{2}{3}\delta_{ij}\sum_l \frac{\partial u_l}{\partial x_l}\right)\right] \quad (3.4)$$

3.2_Reynolds Average Navier Stokes - RANS

Substituting expression 3.1 into the instantaneous continuity and momentum equations and taking a time average yields:

$$\frac{\partial \overline{p}}{\partial t} + \frac{\partial}{\partial x_i}(\overline{\rho u_i}) = 0 \quad (3.5)$$

$$\frac{\partial}{\partial t}(\overline{\rho u_i}) + \sum_j \frac{\partial}{\partial x_j}(\overline{\rho u_i . u_j}) = -\frac{\partial \overline{p}}{\partial x_i} + \sum_j \frac{\partial}{\partial x_j}\left[\mu\left(\frac{\partial \overline{u_i}}{\partial x_j} + \frac{\partial \overline{u_j}}{\partial x_i} - \frac{2}{3}\delta_{ij}\sum_l \frac{\partial \overline{u_l}}{\partial x_l}\right)\right] + \sum_j \frac{\partial}{\partial x_j}(\overline{-\rho u_i^{'} u_j^{'}}) \quad (3.6)$$

Equations 3.5 and 3.6 are called Reynolds Averaged Navier-Stokes (RANS) equations. They have the same general form as the instantaneous Navier-Stokes equations, with the velocities and other solution variables now representing time-averaged values. Additional terms now appear that represent effects of turbulence. These Reynolds stresses, $-\overline{\rho u_i^{'} u_j^{'}}$ must be modeled in order to close Equation 3.6.

The simplest "complete models" of turbulence are two-equation models in which the solution of two separate transport equations allows the turbulent velocity and length scales to be independently determined. **The Standard k - ε model** in some codes falls within this class of turbulence model and has become very popular for practical engineering flow calculations since it was proposed by Launder and Spalding. Robustness, economy and reasonable accuracy for a wide range of turbulent flows explain its popularity in industrial flow and heat transfer simulations. It is a semi-empirical model. Derivation of model equations relies on phenomenological considerations and empiricism. Recently two more models have been derived from the Standard k - ε model. They are called the RNG k - ε and the Realizable k - ε models whose details may be found in CFD handbooks.

The Standard k - ω model is based on the Wilcox k - ω model which is applicable to wall bounded flows. The Shear-Stress Transport (SST) k - ω model developed by Menter is a variation of the Wilcox model. It mixes the robust and accurate formulation of the k - ω model in the near-wall region with the free-stream independence of the k - ε model in the far field. Details concerning the k - ω and SST k - ω models may be found in CFD handbooks.

The Reynolds Stress Model (RSM) is the most elaborate turbulence model that RANS codes may provide. Abandoning the isotropic eddy-viscosity hypothesis, the RSM closes the Reynolds-averaged Navier-Stokes equations by solving transport equations for the Reynolds stresses, together with an equation for the dissipation rate. This means that five additional transport equations are required in 2D flows and seven additional transport equations must be solved in 3D.

Since the RSM accounts for the effects of streamline curvature, swirl, rotation, and rapid changes in strain rate in a more rigorous manner than one-equation and two-equation models, it has greater potential to give accurate predictions for complex flows. However, the fidelity of RSM predictions is still limited by the closure assumptions employed to model various terms in the exact transport equations for the Reynolds stresses. The modeling of the pressure-strain and dissipation-rate terms is particularly challenging and often considered to be responsible for compromising the accuracy of RSM predictions.

3.3_Large Eddy Simulation - LES

Conceptually, LES is situated somewhere between DNS and RANS approaches. Basically large eddies are resolved directly in LES, while small eddies are modeled. The rationale behind LES can be summarized as follows:

- Momentum, mass and energy are transported mostly by large eddies.
- Large eddies are defined by the geometry case and boundary conditions of the flow.
- Instead, small eddies are less dependent on the geometry. They tend to be more isotropic and are consequently more universal.
- It is easier to find a universal turbulence model when only small eddies are modeled.

The governing equations employed for LES are obtained by filtering the time-dependent Navier-Stokes equations in either Fourier (wave-number) space or configuration (physical) space. The filtering process effectively filters out the eddies whose scales are smaller than the filter width or grid spacing used in the computations. The resulting equations thus govern the dynamics of large eddies. A filtered variable (denoted by an overbar) is defined by

$$\bar{\phi}(x) = \int_D \phi(x')G(x,x')dx' \tag{3.7}$$

where D is the fluid domain and G is the filter function that determines the scales of the resolved eddies.

Subgrid scale models

a) The most basic of subgrid-scale models was proposed by Smagorinsky and further developed by Lilly. In the **Smagorinsky-Lilly model**, the eddy viscosity is modeled by

$$\mu_t = \rho L_S^2 \left|\bar{S}\right| \tag{3.8}$$

where L_S is the mixing length for subgrid scales and $\left|\bar{S}\right| \equiv \sqrt{2\bar{S}_{ij}\bar{S}_{ij}}$. L_S is computed using:

$$L_s = \min\left(\kappa d, C_S V^{1/3}\right)$$

where C_S is the Smagorinsky constant, κ is the Von Karman constant, d is the distance to the closest wall and V is the volume of the computational cell.

b) The **Renormalization group (RNG)** can also be used to derive a model for the subgrid scale eddy viscosity. Details may be found in CFD Handbooks.

3.4_Near wall treatment for wall bounded turbulent flows

k - ε and RSM RANS models and the LES model are primarily valid for turbulent core flows (i.e., the flow in the regions somewhat far from walls). Consideration therefore needs to be given as to how to make these models suitable for wall-bounded flows. The Spalart-Allmaras and $k-\omega$ models were designed to be applied throughout the boundary layer, provided that the near-wall mesh resolution is sufficient.

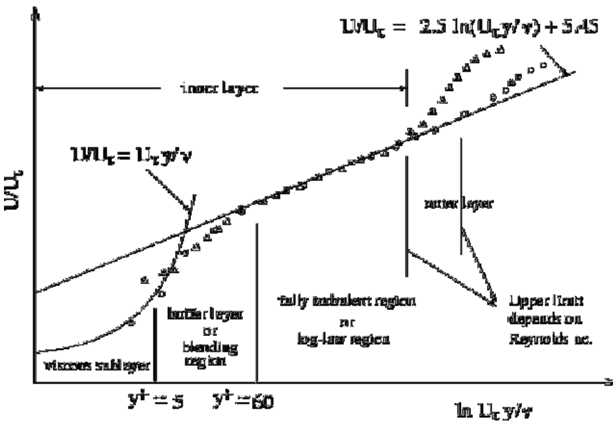

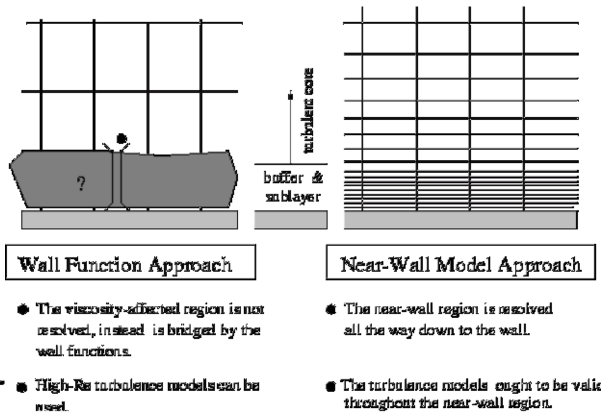

Figure 3.2 (left): Subdivisions of the velocity profile from the viscous layer (wall) to the fully turbulent flow (core) – experimental results with approximate equations.

Figure 3.3 (right): Near wall treatments in fluid codes: Wall function and Near Wall Model Approach. Above illustrations are extracted from a flow code handbook

Numerous experiments have shown that the near-wall region can be subdivided into three layers. In the innermost layer, called the **"viscous layer"**, the flow is almost laminar, and the (molecular) viscosity plays a dominant role in momentum and heat or mass transfer. In the outer layer, called the **"fully-turbulent layer"**, turbulence plays a major role. Finally, there is an intermediate region, the **"buffer layer"** between the viscous layer and the fully turbulent layer where the effects of molecular viscosity and turbulence are equally important. Figure 3.2 illustrates these subdivisions of the near-wall region, plotted in semi-log coordinates.

There are two approaches for modelling / resolving the near wall region. In one approach, the viscosity affected inner region (viscous layer and buffer layer) is not resolved. Instead, semi empirical formulas called “wall functions” (figure 3.3) are used to bridge the viscosity affected region between the wall and the fully turbulent region. One mesh is generally sufficient to cover the totality of the viscosity affected region. The mesh thickness in dimensionless unit is of the order of 30 to 60 (figure 3.2).

In another approach, the turbulence models are modified to enable the viscosity affected region to be resolved with a fine mesh grid. Generally, the mesh thickness in dimensionless unit is of the order of 1 (figure 3.3).

4_Flow simulations_2D structured surfaces_RANS code

4.1_Definition of the simulated flow case

As presented in section 2, structured surfaces may be analysed at any Reynolds number and with any type of channel geometry.

4.1.1 Choice of a Reynolds number

Simulation of structured surfaces could be carried out at gas transport conditions for which the Reynolds number is relatively high (from 10 to 100 millions). This would require an extremely large number of meshes and an extremely long computation time. However, if the same type (shape) of structured surfaces was studied at a reduced Reynolds number, say of the order of 10000, the flow would present similar turbulent characteristics but it would simplify considerably the flow simulation case (computation time millions of time shorter).

As dimensions of structured surfaces are governed by similitude laws (dimensions proportional to the friction length), a simulated case (low Re) may be used to derive the dimensions of structures required for an application case (large Re). It only requires to calculate in each case the friction length, a parameter which is a function of the fluid density, velocity and viscosity and to keep constant the ratio between the absolute structure dimension and the friction length in both Re number cases (high and low).

4.1.2 Choice of channel geometry

Pressure losses in circular and rectangular channels are mostly dependent on the Reynolds number parameter and on wall characteristics (roughness or organised structures). They differ very slightly due to the corner effect in the rectangular channel case generating secondary flows at each corner.

However, the effect of a structured surface is strictly local, of the order of one boundary layer thickness. Therefore, as long as a structured element is analysed at a few boundary layers distance from the corner of a rectangular channel there is no interaction between the two.

The use of a rectangular channel provides a larger density of structured meshes compared to a circular channel which in turn permits to reduce the total number of mesh compared to an unstructured grid.

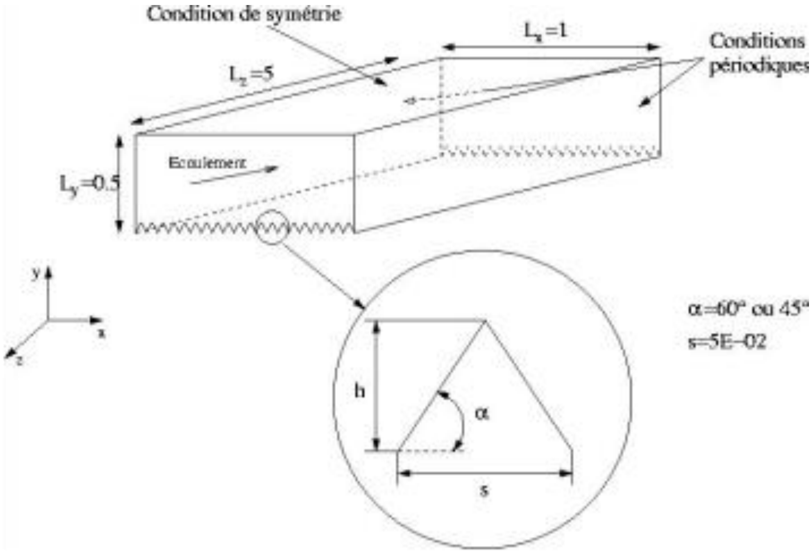

Figure 4.1 – Channel geometry and triangular riblet cross section

To compromise between a preference for a structured grid (rectangular channel) and the detrimental effect of side walls (corner effect) a solution consists in considering a fluid flowing between two plates with an infinite width (figure 4.1). However, the calculation is limited by using a "model width" with a periodicity condition between two fictive side walls. It results that away from these walls, the flow configuration is repeated periodically. The degree of periodicity has no effect on the results. This was demonstrated during the course of the present study by reducing the number of riblets from 20 to 3 then to 1. No change was found in the final result.

The selected dimensions of the channel geometry are the following: physical length, 5m; physical height, 1m (distance from wall to channel axis, 0.5m) and "model" width, 1m.

4.1.3 Flow conditions

- Pressure : 1 bar, temperature, 300 °K
- Density : 1.6 kg/m^3
- Viscosity : 2.27*10^{-5} Pa.s

4.1.4 Triangular riblets

Two types of triangles with relatively optimized shapes have been studied. Angle α is, respectively, 45° and 60° (figure 4.1).

Angle α = 45°, Riblet width (S) = 0.05 m; Riblet height (H) = 0.025 m

Velocity – m/s	0.05	0.1	0.2
Reynolds	7040	14000	28100
Riblet width – S^+ (1)	11.6	21.2	38.9
Riblet height – H^+ (1)	5.8	10.6	19.5
Size of wall mesh–m	0.0043	0.0024	0.0013

Angle α = 60°, Riblet width (S) = 0.05 m; Riblet height (H)= 0.0433 m

Velocity – m/s	0.05	0.1	0.2
Reynolds	7040	14000	28100
Riblet width – S^+ (1)	11.6	21.2	38.9
Riblet height – H^+ (1)	10.0	18.4	33.7
Size of wall mesh–m	0.0043	0.0024	0.0013

(1) dimensionless width and height : actual dimension divided by friction length

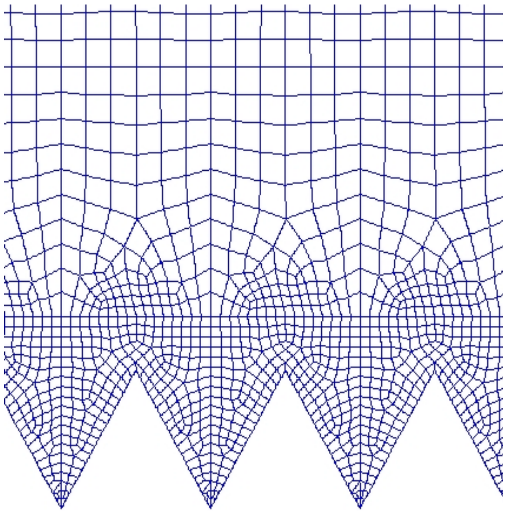

Figure 4.2 – Mesh grid for fluid flow section – Case of triangular riblets

4.2_Turbulence models

Three turbulence models (section 3.2) have been tested during the course of flow simulations:

- the k - ε model,
- the k - ω model,
- the RSM model

These models have been tested as well for evaluating the channel friction factor as for analysing the secondary flow occurring near a structured surface.

4.3_Triangular riblets – Effect of triangle shape

Results of the flow simulations obtained with the k - ε model are presented on figure 4.3 for two cases of angle (45° and 60°) of triangular riblets.

Simulation results (flow drag reduction versus the adimensional riblet spacing) are relatively similar to the experimental results of K.N.Liu et al. (1986 – figure 2.5). The maximum drag reduction is of the order of 6% in both cases. Maximum drag is obtained in the present simulation case for S^+=18 while Liu found 13 and the drag reduction becomes nil when S^+ is slightly greater than 42 while Liu found a value of the order of 22.

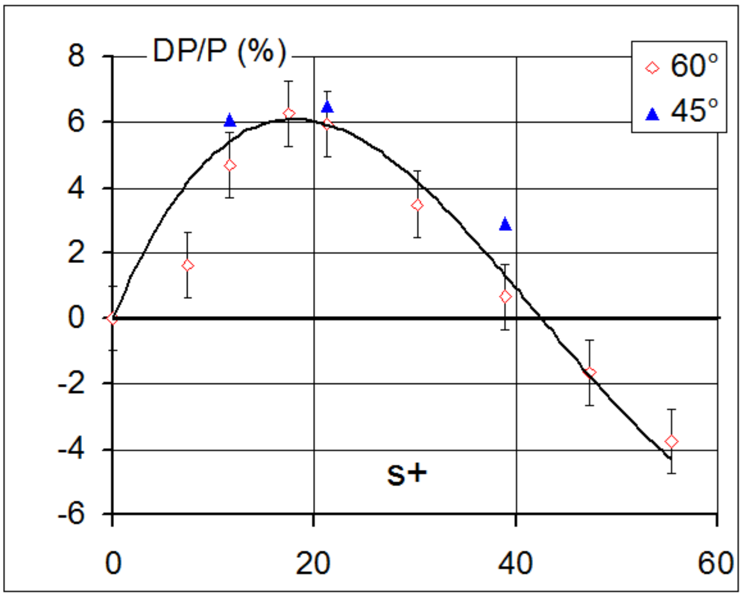

Figure 4.3 – Drag reduction in per cent versus dimensionless riblet spacing

Except for the shifting in the S^+ parameter, the same trend is observed in both cases (Liu experiments and the present RANS study) that is a drag reduction which increases from 0 (S^+=0 representing the smooth flow case), passing through a maximum drag reduction (riblet adapted to the fluid flow) then follows a progressive decrease in drag reduction. In both cases, the point where the drag reduction is nil corresponds to a flow which is approximately twice the one corresponding to the maximum drag reduction.

Explanation for the shifting in S^+ (dimensionless width) or Q^+ (dimensionless flow) may be found considering, possibly:

- a difference in roughness of structure walls (partially rough walls in experiments against fully smooth walls in theoretical studies),
- a different definition in hydraulic diameter (Liu using a circular pipe and flow between two plates in the present simulation),
- an effect of the turbulence model,
- a different definition in the fluid velocity (average versus peak velocity values).

The effect of the triangular shape was analysed in varying the triangular angle from 10 to 80° (figure 4.4). Simulation results are presented on figure 4.5.

As expected from the literature, the maximum drag reduction is obtained for an angle ranging in between 45 and 60°. Below and above that range, the maximum drag reduction is smaller due to the progressive disappearance of the solid structures (structures tending towards a smooth surface, the fluid flow being aligned with the riblets).

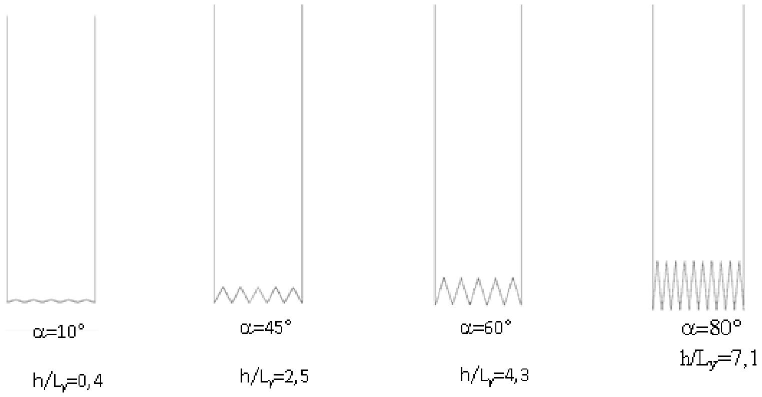

Figure 4.4 – Triangular riblets with angle varying from 10 to 80 degrees

There is however, a significant difference between the 10 and 80° angle cases:

- in the 10° angle case, the amplitude of the triangle is relatively small. If the angle was further reduced, the amplitude would tend towards 0 and the triangles would tend to the smooth surface of reference.
- in the 80° angle case, the amplitude of the triangle is relatively large. If the angle was further increased, the amplitude would tend towards infinite and the triangles would tend to a smooth surface with a considerably smaller hydraulic diameter. In these circumstances, the actual performance of a riblet needs to be determined in using riblets with smaller amplitude (study carried out at a larger Reynolds number) or the actual hydraulic diameter has to be calculated to get the proper reference for the smooth surface.

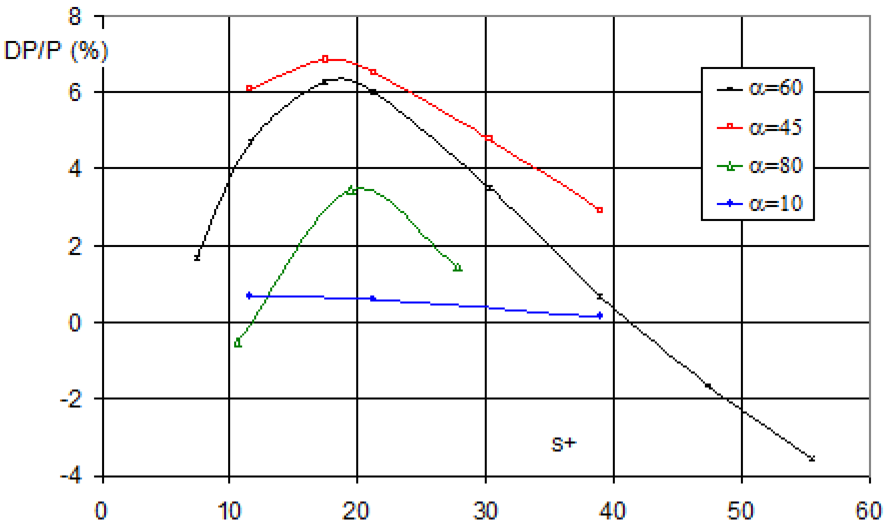

Figure 4.5 – Drag reduction for triangular riblets with angles varying from 10 to 80°

4.4_Triangle and knife blade riblets

The performance of triangular and knife blade shape riblets have been compared. Results are presented on figure 4.6.

As mentioned in the literature, knife blade shape riblets provide twice more drag reduction compared to triangular riblets. The maximum drag is obtained for the same S^+ values considering that the absolute spacing is the same in both cases.

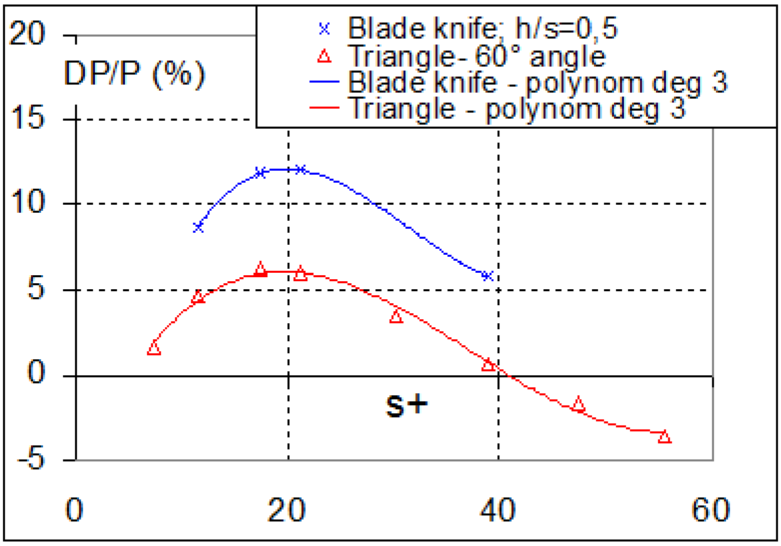

Figure 4.6 – Drag reduction for triangular (60° angle) and knife blade shape riblets

4.5_Secondary flows around triangle riblets

Secondary flows occurring around solid structures could not be obtained with k - ε nor the k -ω models (isotropic models). Only the RSM model (anisotropic model) provides secondary flow information.

Figures 4.7 and 4.8 compare results of flow simulations carried out in DNS (S+= 40 and 20) by H. Choi et al. (1993) and of flow simulations carried out in the present study in RANS (S+=21). These figures represent, respectively, the velocity field and the vorticity in the transverse plane (perpendicular to main flow).

As it can be seen from these two figures, similar behaviour of secondary flows is observed with DNS and RANS (RSM model) codes.

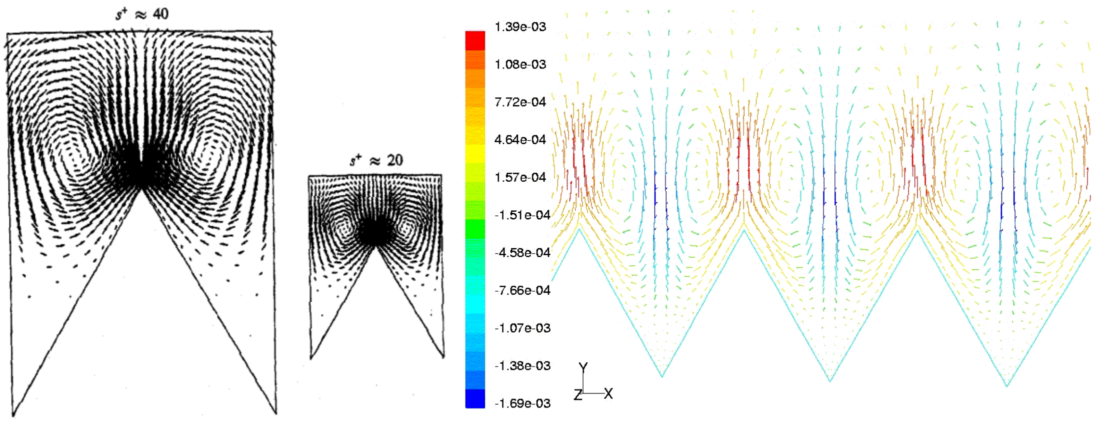

*Figure 4.7 – Transverse secondary flow around triangular riblets - **Velocity field** – Comparison between DNS work by H. Choi et al. (1993-left) and RANS simulation with actual work (right)*

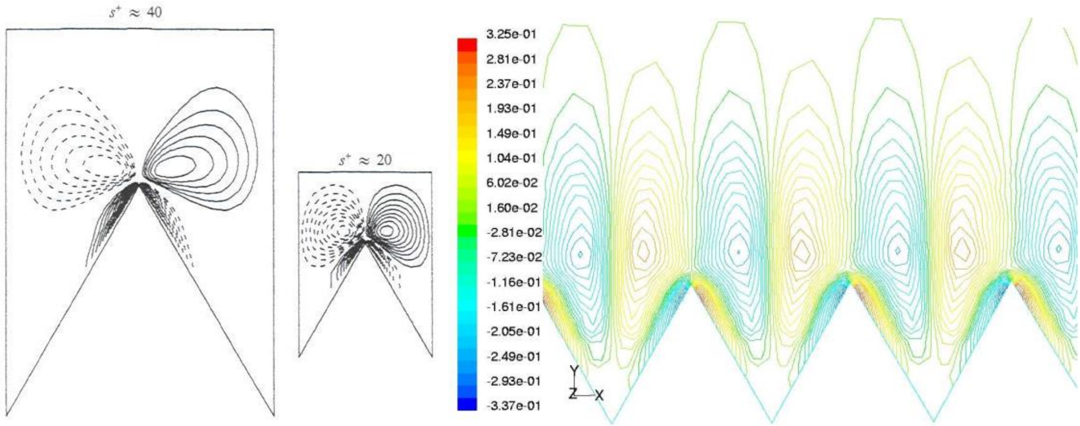

*Figure 4.8 – Transverse secondary flow around triangular riblets – **Vorticity** – Comparison between DNS work by H. Choi at al. (1993-left) and RANS simulation with actual work (right)*

5_Conclusions

RANS codes, based on turbulence modelling (**k - ε model**), can be used to determine the degree of drag reduction of a specific riblet type versus its relative dimensions (or relative flow).

These codes may be used for flow drag comparison between different riblet types and for determining the optimum shape and optimum dimensions of 2D riblets.

The maximum flow drag reduction is obtained with knife blade riblets with a dimensionless interval S^+ of 18. The maximum value is 12 per cent. The maximum value is only of 6 per cent in the case of structures with triangle shape with angles of 60 degrees. These data are confirmed by the results quoted in previous research works.

Only the RSM turbulence model has been identified for providing suitable information on transverse secondary flows near structured surfaces.